NASA Technical Memorandum 89439

Aerothermodynamics Research at NASA Ames Research Center

George S. Deiwert

September 1987

NASA

National Aeronautics and
Space Administration

Aerothermodynamics Research at NASA Ames Research Center

George S. Deiwert, Ames Research Center, Moffett Field, California

September 1987

NASA

National Aeronautics and
Space Administration

Ames Research Center
Moffett Field, California 94035

SUMMARY

Research activity in the aerothermodynamics branch at the NASA Ames Research Center is reviewed. Advanced concepts and mission studies relating to the next generation aerospace transportation systems are summarized and directions for continued research identified. Theoretical and computational studies directed at determining flow fields and radiative and convective heating loads in real gases are described. Included are Navier-Stokes codes for equilibrium and thermochemical nonequilibrium air. Experimental studies in the 3.5-ft hypersonic wind tunnel, the ballistic ranges and the electric arc driven shock tube are described. Tested configurations include generic hypersonic aerospace plane configurations, aeroassisted orbital transfer vehicle shapes and Galileo probe models.

INTRODUCTION

Current research activity in the Aerothermodynamics Branch at the NASA Ames Research Center is outlined and described. Focused activity is directed toward orbiting high-altitude, high-drag aerobraking vehicle configurations such as aeroassisted orbital transfer vehicles (AOTVs). and high-lift transatmospheric vehicles (TAVs) for the purpose of maturing the enabling technology necessary for the design of such vehicles. Research efforts are divided into four distinct areas: 1) advanced mission and concept studies, 2) computational aerothermodynamic flow-field code development, 3) thermochemical non-equilibrium reacting gas models. and 4) code validation experiments. These four research areas are considered synergistically to extend the state of the art in aerothermodynamic technology.

Advanced mission and concept studies identify the thermal-control requirements for design-optimized, aeromaneuvering performance for space-based applications and low-Earth orbit (LEO, 400 km altitude) sorties involving large. multiple plane-inclination changes. Heating analyses for hypersonic, low-density viscous flows including real-gas chemistry and surface catalysis are considered. The predicted aerothermodynamic heating characteristics are correlated with thermal-control and flight-performance capabilities. Mission payload capability for delivery, retrieval. and combined operations is determined for round trip sorties extending to polar orbits. The results help to identify technology issues required to develop prototype operational systems. and to provide guidance and direction for development of computational aerothermodynamic flow codes.

The design of the next generation aerospace transportation systems will be driven by considerations such as fully reusable systems, maximum payload-to-total-weight ratios

1

and high-altitude aeromaneuverability to achieve orbital plane change and cross-range capability. These considerations, and others, will be finely tuned to effect designs for economically viable vehicles such as rapid-response TAVs and space freighter concepts like the AOTV.

In the past heavy reliance was made using ground-based test facilities such as shock tubes, arc jets, and ballistic ranges, in conjunction with engineering design and analysis codes, to achieve closure on designs of such vehicles as the Apollo, the Space Shuttle, and the Galileo probe. Many of these vehicles were expendable "one-shot" vehicles that use ablative heat-shield materials. The space shuttle, a reusable nonaeromaneuvering vehicle, employs reusable tiles but must undergo considerable refurbishment between missions. To design fully reusable aeromaneuvering vehicles will require design tools significantly improved over those used in the past, and design tolerances will need to be much tighter to avoid unnecessary weight penalties that can drive the cost beyond economic viability.

Ground-based test facilities can provide valuable insight for the design and understanding of aerospace vehicles. Such facilities, however, cannot simulate all of the conditions that will be encountered in planned missions of the future. Shown in figure 1 is the flight domain for a variety of aerospace vehicles for typical missions in terms of flight Reynolds number and flight Mach number. Superposed are regimes which can be simulated by typical ground-based test facilities. The high-altitude, high-speed regime is the most difficult to simulate, yet it is this regime that will be encountered by vehicles of the future. Flight tests can, and are being planned, such as the aeroassist flight experiment (AFE), to provide data in this regime. But these tests are expensive and can provide only a limited amount of data. To augment this data and to optimize cost-effective designs, reliance must be made on advanced computational techniques. Both ground-based and flight tests can provide valuable data to validate these computational methods. The computational methods can then, in turn, be used to extrapolate our understanding and analysis in to regimes not covered by existing facilities.

Over the past decade and a half, during the hiatus in hypersonic research, we have seen great advances in three key areas that are now being synthesized to develop advanced computational techniques to a mature technology to enable the design of the next-generation aerospace transportation systems. The first of these is the development of inexpensive raw computing power. In the early 1970s, scientific computers were of the IBM 360 and CDC 6600 class. The IBM 370 series and CDC 7600 machines were just becoming available. Since that time we have seen the Cray 1 and Cray 2 computers, the CDC Cyber 205 and the Fujitsu VP200 and VP400 and Hitachi S 810. Coming along are the ETA 10 and the Cray 3 supercomputers. These computers are faster in terms of computing speed and larger in terms of high-speed memory by orders of magnitude and, at the same time, cost is orders of magnitude less per unit of computing power than a computer of a decade and a half ago.

During the same period a new and powerful tool in aerodynamics was developed; computational fluid dynamics (CFD). Numerical algorithms have been refined to efficiently solve the Reynolds-averaged Navier-Stokes equations for three-dimensional (3-D) steady and unsteady compressible flows at transonic and supersonic speeds in an ideal gas. Associated with this are sophisticated discretization schemes to describe complex geometries and

flow fields. To extend the CFD capability to the hypersonic flight regime experienced by aerospace vehicles it is necessary to include "real-gas" effects. Typically this involves the description of chemical reactions, thermochemical nonequilibrium and radiative transport phenomena.

At the very high temperatures associated with high-altitude hypervelocity flight there is a paucity of experimental data defining collision cross-sections and transition probabilities necessary to accurately describe the chemical exchange processes involved. To this end, recent advances in computational chemistry can be used to fill this critical gap. A recent survey describing the capability of computational chemistry and the impact on the analysis of orbital transfer vehicles is given by Cooper et al. (ref. 1). The combination of CFD and real-gas chemistry, along with modern high-speed computers form the synergistic basis of computational aerothermodynamics (CAT). Three excellent recent review articles on computational aerothermodynamics are given by Anderson (ref. 2), Graves and Hunt (ref. 3), and Lewis (ref. 4).

The particular phenomena addressed by computational aerothermodynamics is the prediction of aerothermal loads. These include effects such as aerodynamic forces, convective and radiative heating rates, gas/surface interactions and surface catalytic effects, thermal protection systems (TPSs) with active cooling and plasma layers and their effect on communications and power supply. These phenomena are critical to designing vehicles that are to be adequately protected from the very high thermal loads that will be encountered during hypervelocity flight and that are to be aerodynamically stable and maneuverable. Existing ground-based test facilities will be used to perform critical experiments designed to provide data for real-gas computer-code validation.

ADVANCED MISSION AND CONCEPT STUDIES

In conceptual studies extending over the past two decades (refs. 5-7), the potential of aeroassisted technology for enhancing orbital operations and planetary missions has been widely recognized. This technique calls for using the aerodynamic forces produced by grazing passes through the upper atmosphere to achieve the transition to local orbit by deceleration or directional change; earlier methods relied exclusively on propulsion power. The propellant saved by eliminating the costly propulsive maneuvers not only makes possible missions that are otherwise impractical but also substantially increases payload capability. Exploratory studies (ref. 7) have indicated that two classes of AOTVs can satisfy a broad range of Earth-centered, space transport missions.

Aerobraking AOTVs

One design, useful primarily as a space freighter for transporting large payloads when time is not a constraint in the mission requirements, is aerobraking AOTVs. Aerobraking vehicles perform its orbit-change maneuvers by aerodynamic drag in the far-outer extent of the atmosphere to alleviate surface heat fluxes and pressure forces, therefore minimizing the weight penalties for the aeroassist apparatus. Extensive design and mission-performance analyses for operations encompassing cislunar space have been given by Menees et al.

3

(refs. 8, 9) and Davies and Park (ref. 10) for an AOTV design in this category. A typical near-Earth orbital transfer mission would be between a geosynchronous Earth orbit (GEO, 35,841 km altitude) and an equatorial LEO. The location of a space station at GEO is a future certainty because of its many scientific, commercial, and strategic applications. Consequently, low-cost orbital-change maneuvers between GEO and LEO (or Space Shuttle orbits) for personnel and material transport will be a future requirement of high frequency. The advantages of aerobraking provide substantial savings in propulsion fuel mass for this mission. This is illustrated in figure 2 by a typical mission profile for a single-pass, AOTV maneuvering between GEO and equatorial LEO. Multiple passes are possible and appropriate for unmanned missions for which turnaround time is unimportant, but a single pass is appropriate for manned missions. The constraints on the mission are a re-entry mass of 12 tons (to conform with other studies) and the use of a liquid rocket engine with a specific impulse of 420 sec to make the AOTV reusable and refuelable. The mission scenario is as follows: 1) the AOTV with initial mass of 30 tons (the approximate capacity of Space Shuttle cargo bay) is inserted into equatorial LEO; 2) a propulsive thrust of 2395 m/sec is required to transfer from the circular LEO to an elliptical orbit with apogee at GEO and perigee at LEO; 3) this consumes a propulsion fuel mass of about 45% of the initial AOTV mass; 4) a propulsive thrust of 1456 m/sec is required to achieve the circular GEO from the elliptical transfer orbit; 5) this maneuver consumes an additional 30% of the AOTV mass; 6) a payload of 5.5 tons is picked up for transfer to LEO so that a re-entry mass of 12 tons will be obtained subsequently; 7) a retropropulsive thrust of 1490 m/sec is required for transfer to an elliptical orbit with perigee in Earth's atmosphere to take advantage of aerodynamic braking; 8) this maneuver expends 30% of the remaining AOTV mass in fuel and provides the desired re-entry mass of 12 tons; 9) aerodynamic braking occurs with the AOTV, achieving a new elliptical orbit with apogee at LEO; and 10) a final small propulsive thrust of 90 m/sec is required for insertion into LEO, which burns a fuel mass of only 2.5%. Thus, aerobraking conserves essentially all of the fuel mass that would be required for return to LEO using all-propulsive maneuvers, which is about 45% of the AOTV mass (the difference between propulsive thrust for steps 2 and 10).

Several design concepts have been considered for orbital transfer vehicles including a conical lifting-brake (refs. 5, 11), a raked elliptic-cone (refs. 12, 13), a raked sphere-cone (ref. 14), a lifting body (ref. 15), and a ballute. These five concepts have recently been reviewed and critiqued by Park (ref. 16). Historical backgrounds, and the geometrical, aerothermal, and operational features of the designs are considered as are the technological requirements for the vehicle (namely, navigation, aerodynamic stability and control, afterbody flow impingement, nonequilibrium radiation, convective heat-transfer rates, mission abort and multiple atmospheric passes, transportation and construction, and the payload-to-vehicle weight requirements). These issues are delineated and recent advances that have been made in them are summarized. Each of the five design concepts are critiqued and in table 1 are rated on these issues. The highest and the lowest ratings are given to the raked sphere-cone and ballute designs, respectively. A fairly indepth aeroelastic analysis of the bottom-rated ballute concept is given by Park (ref. 17) which identifies critical concerns with aerodynamic stability.

The highest-rated sphere-cone concept is described in detail by Davies and Park (ref. 14) and is illustrated in figure 3. To position the thrust line correctly, the two rocket engines must exhaust forward through an opening in the aerobrake as seen in figure 3a. The thrust line in each of the two engines passes through the approximate center of gravity (c.g.) at take-off (fig. 3c) so that, in case one engine fails, there would be no unduly large yawing moment. The engines have telescopic extensions that serve two purposes: prevent spilling of rocket exhaust gas behind the aerobrake, and increase nozzle area ratio and thereby thrust. Two hinged hatches must be provided on the aerobrake for the telescopic engines and are indicated in figure 3c. Similar hatches are already incorporated into the Space Shuttle for its landing gear. Two sets of fuel tanks exist in this design: the main tanks within the heavily armor-protected command/control module, and the auxiliary tanks dispersed behind the aerobrake as seen in figure 3b. The fuel in the auxiliary tanks will be used first; the fuel in the main tanks (comprising 5-10% of the total fuel capacity) will be kept as a reserve. The heavy oxygen tanks are located on the central yaw plane to minimize their effect on the trim angle. The tanks for the much lighter liquid hydrogen are located symmetrically on the central pitch plane so that possible imbalance in the amounts of hydrogen in the two tanks would not greatly affect the trim angle of attack. In case one engine fails, oxygen can be shifted from one auxiliary fuel tank to the other to realign (in the yaw plane) the c.g. with the thrust line of the functioning engine. The toroidal-shaped main oxygen tank inside the command/control module has four compartments. Large adjustments in the c.g., if needed during operation of the rocket engines or during atmospheric flight, can be made by shifting liquid oxygen among these four compartments. Fine adjustments in the c.g. during the atmospheric flight can be performed by gimballing the engines.

On the base side of the aerobrake, the command/control module and the auxiliary fuel tanks are covered by a shroud (fig. 3a) made of lightweight heat-shield material. The shroud serves three purposes: first, it thermally protects the auxiliary fuel tanks and the command/control module from the hot recirculating flow in the base region; secondly, it protects the tanks from possible meteoroid bombardment; and thirdly, it is used as a radiating surface for the thermal control of the components it encloses. The cargo bay has a two-part shield (seen open in fig. 3c) which also serves three purposes. First it thermally protects the payload; second, it protects the cargo from meteoroid bombardment; and third, in case of failure of one engine, it can serve as a ballast (that is, by opening one shield, the c.g. shifts in the yaw plane which brings the c.g. closer to the thrust line of the functioning engine).

High-Lift AOTVs

The other generic AOTV design is a very high-lift "aeromaneuvering" vehicle. This is an essential operational requirement if time-constrained, aeroassisted maneuvers are to be accomplished between LEOs involving large, multiple plane-inclination changes. Such high-lift vehicles serve as space taxis. They achieve rapid response from one orbital plane to another but have the inherent liability of small payload fraction because of low volumetric efficiency.

Results were given by Menees (refs. 7, 9), Davies and Park (refs. 10, 11), and Brown (ref. 18) of detailed system-design studies for configurations in the high-lift AOTV category. These were the first studies to address the problem of rarefied-hypersonic flow over a lifting surface at incidence with the inclusion of appropriate viscous/inviscid interaction phenomena. A subsequent work by Menees (ref. 19) brings together the diverse details of the research activities at NASA Ames Research Center for high-lift AOTVs and is an adjunct to this paper. Special emphasis is given to the problems of hypervelocity, low-density, viscous effects on flow-field dynamics and thermochemical relaxation effects.

The use of high-lift vehicles when returning from LEO has many advantages. A primary benefit of lift is the ability to achieve large longitudinal range. Lift also provides the capability to maneuver within the atmosphere. Maneuver ability enhances mission flexibility and increases the choice of landing sites. Lift can also be used to alleviate the deceleration loads and aerodynamic heating which accompany atmospheric entries. The resultant moderation of the entry environment benefits the vehicle's occupants and permits lower-structural and thermal protection weights. Skipping flight paths can be used to maximize both longitudinal and cross ranges (Menees et al. Submitted to AIAA 26th Aerospace Sciences meeting, Reno, NV, Jan. 1988) but have associated with them adverse deceleration, structural load factors and aerodynamic heating factors when compared with gliding flight paths (ref. 20). Even for entry angles of less than 10°, the deceleration loads can be an order of magnitude higher for skip flight paths; therefore the crew of a skipping vehicle experiences severe physiological stress. To withstand the increased structural loads, such major components as the fuselage and wings must be two to three times heavier. Heating rates are four to five times higher and require heavier TPSs.

Air-Breathing TAVs

The developing need for more economical access to space has spurred renewed interest in TAVs in both the United States and Europe. Such a TAV would have responsive, flexible operational characteristics approaching those of aircraft and might eventually replace the Shuttle by providing short launch notice and turnaround times. The TAV would be able to take off and land from ordinary runways and operate in LEOs. A lower-speed variant of such a vehicle may be used to transport passengers or high-value cargos to any location on the Earth in a small fraction of the flight time of current jet airliners.

The configurations proposed for TAVs would use primarily air-breathing propulsion systems (scramjets) for extended periods of hypervelocity flight to orbital speed. The hypervelocity flight within the atmosphere subjects the vehicle to severe aerodynamic heat fluxes and total heat loads. Therefore the thermal protection of such vehicles will be major design considerations. A TAV using air-breathing propulsion must fly in the denser part of the atmosphere to achieve adequate acceleration to reach orbital speed. The elements of severe aerothermodynamic environment are therefore coupled with the requirement of low aerodynamic drag. To achieve low drag, the vehicle must be slender and must have a relatively sharp nose and wing leading edges. Propulsion and aerodynamic performance of typical TAVs were approximated and trajectory and angle of attack histories were derived which allow meaningful computation of the surface heating rates and heat loads (refs. 21, 22). Heating rates, equilibrium wall temperatures, and total heat loads at the stagnation

6

point, along a postulated wing leading edge and on the windward surface centerline of the vehicle are presented.

The combination of high heating rates experienced by surfaces with small curvatures and the long ascent times results in large total heat loads. Therefore the most severe heating occurs during ascent at the stagnation point and wing leading edges. In contrast, atmospheric entry occurs at large angles of attack, since high drag is desirable to reduce the length of the heating pulse. A comparison of total windward centerline heating loads for typical ascent and entry trajectories (ref. 22) are shown in figure 4. Temperatures peak around 1300° K during both ascent and entry and radiative cooling should be effective over large areas of the vehicle. Ascent-peak stagnation point and wing leading-edge wall temperatures are about 3500° K and 2500° K, respectively. Therefore some form of active cooling may be required for these regions of the vehicle. The corresponding temperatures during entry are 1000° K lower.

COMPUTATIONAL AEROTHERMODYNAMICS

Computational fluid dynamics involves the numerical simulation of the equations of motion for an ideal gas: these equations are the conservation of mass, momentum and energy. In their most general form these equations are the compressible Navier-Stokes equations. For turbulent flows the range of length scales is too great to feasibly be resolved numerically, and so these equations are time averaged over a scale small with respect to the mean motion time scale yet large with respect to the fine-scale turbulent structure. These small-scale turbulent transport processes are modelled using eddy viscosity and eddy conductivity concepts. Many flow fields have been well simulated for a variety of shapes and flow conditions where strong viscous/inviscid interactions and/or flow separation are important by solving these equations in a time-like manner until a steady state is asymptotically achieved. When there is no flow reversal and the flow in the streamwise direction is supersonic these equations can be simplified by neglecting the streamwise viscous terms. The solution to these simplified equations, referred to as the parabolized Navier-Stokes equations, can be found by efficient streamwise marching techniques. Further simplification can be achieved when viscous/inviscid interactions are weak by decoupling the viscous and inviscid dominated regions from one another and simulating the regions separately in an iterative manner. Here the inviscid Navier-Stokes equations, termed the Euler equations, and are solved in the inviscid region away from body surfaces. Near the body surface the viscous-dominated boundary-layer equations are solved. A fourth simplification which can be used for strong viscous/inviscid interactions is the viscous shock-layer (VSL) approximation. The VSL equations are obtained from the steady-state Navier-Stokes equations by retaining terms up to second order in the inverse square root of the Reynolds number. In addition, approximations are invoked for the normal pressure gradient and the bow-shock location.

These four equation sets: Reynolds-averaged Navier-Stokes, parabolized Navier-Stokes, Euler plus boundary-layer, and VSL, are used in computational aerothermodynamics to simulate aerothermo loads for a variety of vehicles and flight conditions. Examples of each will be described later along with the influence of real-gas effects.

7

Real-gas effects include thermochemical nonequilibrium, where finite-rate processes for chemical and energy exchange phenomena occur, and radiative transport. To account for chemical reactions, conservation equations for each chemical species must be added to the flow-field equation set. There are five flow-field equations; one continuity, three momentum, and one energy equation. For dissociating and ionizing air there are typically nine species (N_2, O_2, N, O, NO, O^+, N^+, NO^+, e^-). The inclusion of conservation equations for each of these species nearly triples the number of equations to be solved. When there are combustion processes or gas/surface interactions or ablation products, the number of species increases dramatically. To account for thermal nonequilibrium and radiative transport there are additional energy equations to describe the energy exchange between the various energy modes (translational, rotational, vibrational, electronic, etc.) To further complicate the analysis the range of time scales involved in thermochemical processes is many orders of magnitude wider than the mean-flow time scale. This is the single most complicating factor in computational aerothermodynamics. A wide variety of simplifications are used to alleviate problems associated with widely disparate time scales and are discussed briefly next.

Many flows can be adequately approximated by assuming an equilibrium real gas. Here the reaction rates are assumed to all be fast enough that the gas is everywhere in local equilibrium and the thermochemical state of the gas can be defined solely by the local temperature and pressure. Reactions are allowed to occur but are completely uncoupled from the flow-field equations. This is a good approximation for lower altitudes and can be used for a major portion of the analysis of such vehicles as transatmospheric vehicles. In the other extreme, reactions are sometimes so slow that the gas can be considered frozen in a particular chemical state. This phenomenon typically occurs in regions of rapid expansion such as in jets or base regions of body shapes, but can sometime be used behind compressive shocks as well.

When finite rate chemical reactions are important they can often be considered to be in thermal equilibrium. That is, that the energy modes of the species equilibrate very rapidly compared to the chemical rate processes. Even with this simplification the time scales vary over an extremely wide range, resulting in a "stiff" behavior of the complete equation set and adding to the difficulty in solving the flow-field and species equations in a fully coupled manner. In these cases the species equations are often effectively uncoupled from the flow-field equations and solved separately in a "loosely" coupled manner, often by a different (typically implicit) numerical technique.

VSL Methods

Recent applications using VSL techniques are describe in references 18 and 24 - 26. Green et al. (refs. 24, 25) obtained VSL solutions for the forebody of the Titan atmosphere entry probe which is planned to make scientific measurements in the organic haze layer of Saturn's largest moon. The flow was assumed to be in local thermochemical equilibrium and corresponded to an entry velocity of 12 km/sec. Both radiative and convective heating analyses were performed in order to identify the TPS requirements and associated material response necessary to protect the probe. Shown in figure 5 is the chemical species distribution predicted along the stagnation streamline in the forebody shock layer at a time

8

corresponding to the peak heating pulse. The convective and radiative stagnation-point heating histories are shown in figure 6. The heating pulse occurs in the hypersonic, low Reynolds number region of the trajectory and at the stagnation point the peak flux is 2.5 MW/m². A stagnation-point convective-heating correlation was developed from the results of this study which can be employed in approximate heating analyses.

Balakrishnan et al. (ref. 26) solved the radiative VSL equations to analyse the flight data from several experiments including Fire II, Apollo 4, and PAET and compared the computed results with radiometric data from the flight tests. Calculated convective heating rates were found to compare well with experiment, but self-absorbtion and thermochemical nonequilibrium effects precluded good agreement with the radiative heating rates.

In an attempt to account for thermochemical nonequilibrium, Brown (ref. 18) solved the VSL equations for dissociating nitrogen for typical flight speeds of 10 km/sec, altitudes of 80 km and bodies with nose radii from 1 to 50 cm. A two-species, two-temperature nonequilibrium gas model (refs. 27, 28) was assumed and comparisons are made with previous theories, experimental data, and results based on the thermodynamic equilibrium assumption. Results shown in figure 7, in which heat-transfer rate coefficient C_h is shown as a function of rarefaction parameter K_r^2, indicate that the inclusion of vibrational relaxation has little effect on the convective heat-transfer rate for a fully catalytic surfaces but can contribute to increased heating rates to catalytic surfaces. Preliminary studies (refs. 7, 29) indicate that peak heating for a TAV occurs at rarefaction parameter values, K_r^2, between 8 and 18 for a leading edge radius of 10 cm. If low-catalytic materials are used for thermal protection, vibrational nonequilibrium effects will be critical in the structural design.

The effect of thermochemical nonequilibrium on radiative heating has been addressed by Park (refs. 30, 31). The results of these studies indicate that radiative heating loads for typical AOTV missions are of the same order as the convective heating loads.

Euler Methods

Recent applications using Euler methods are described in references 32-36 (Also Palmer, G. E., Submitted to AIAA 26th Aerospace Sciences Meeting, Reno, NV, Jan. 1988). A total variational diminishing (TVD) numerical scheme for high Mach number flows in chemical equilibrium with emphasis on improved convergence is discussed in references 32-34. Here TVD numerical dissipation and real-gas properties are added to one-dimensional (1-D) and axisymmetric codes using the Beam and Warming central-difference algorithm. Solutions are generated for hemispheres and cylinders at Mach 15 and 20 km altitude. Equilibrium solutions were generated for axisymmetric and two-dimensional (2-D) spheres and cylinders at Mach numbers up to 15. The altitude (20 km) and velocities were chosen to reflect the flight regime of hypervelocity atmospheric aircraft. The algorithm uses a TVD dissipation operator which allows strong shocks to be captured. Real-gas properties are provided by the Gordon and McBride (ref. 37) equilibrium chemistry package. Particular attention was devoted to achieving quadratic convergence, which no other equilibrium code has been capable of duplicating. Density and temperature contours show the effect of real-gas chemistry on shock stand-off distance and adiabatic wall temperature. A converged solution gives confidence that the method is stable and correct. In the 1-D code

(Ref. 32) fully coupled finite-rate chemistry is considered in the simulation of hypersonic flow through a strong normal shock.

Yang (ref. 35) solved the 2-D unsteady Euler equations to simulate the impingement of an oblique blast wave on a 2-D AOTV-like configuration. A time-accurate hybrid upwind algorithm was used. Shown in figure 8 is the geometry and computational grid used for the simulation, and in figure 9 are computed Mach number contours for a Mach 30 impinging shock at 15° incidence to the body. These results were computed assuming a frozen gas with $\gamma = 1.1$.

Three-dimensional simulations for equilibrium air are described by Balakrishnan et al. (ref. 36). Thermodynamic properties are evaluated at each computational grid point using an equilibrium composition method (ref. 37) and the code has been validated through detailed comparisons with tabulated data of reference 38. Results were computed for Mach numbers of 10, 15 and 20 at entry altitudes of 20 and 50 km for a hemispherical blunt body with nose radius corresponding to the Space Shuttle.

Parabolized Navier-Stokes Methods

Recent applications using the parabolized Navier-Stokes equations are described in references 39-43. Rakich et al. (ref. 39) solved the equations in 3-D for a Space Shuttle configuration in ideal air. Balakrishnan (ref. 40) and Prabhu and Tannehill (ref. 41) added equilibrium real-air properties. Shown in figure 10 is a comparison of computed temperature distributions for one cross-sectional plane for both ideal and equilibrium air. The real-gas temperatures are significantly lower than the ideal gas temperatures at these flight conditions. Prabhu has extended this capability to include chemical nonequilibrium in 2-D (ref. 42) and 3-D (ref. 43). The gas dynamic and species concentration equations are solved in a coupled manner using a noniterative, implicit, space-marching finite-difference method. The conditions for well-posedness of the space-marching method have been derived from an eigenvalue analysis of the governing equations. Hypersonic laminar flow of chemically reacting air over cones and wedges has been simulated and the results validated. Shown in figure 11 are computed oxygen and nitric oxide species concentrations in the shock layer of a 10° cone for two different altitudes and a speed of 8.1 km/sec. The results compare favorably with reacting boundary-layer results (ref. 44).

Navier-Stokes Methods

Recent applications using Navier-Stokes methods are described in references 45-50. These hypersonic applications are based on two well-established codes. The first, the ARC2D/ARC3D codes, have been applied and validated for a variety of complex configurations and flow fields. Equilibrium air properties are included to enhance the codes to apply to hypersonic flight. The central-difference Beam-Warming algorithm is enhanced by adding TVD modifications so that strong discontinuities can be adequately treated in an upwind-like manner. The second, conservative supra-characteristic method (CSCM), is an upwind scheme developed for hypersonic applications. Equilibrium air properties are included for realistic simulation at flight conditions. Shown in figure 12 are computed concentrations of nitrogen for a Mach 20 flow of equilibrium air over a hemisphere forebody (ref. 46). These results compare well with the results of reference 38.

Of particular importance in the simulation of complex hypersonic flow fields is the ability to adapt the grid to the solution itself. Two codes, ADAPT2D and ADAPT3D are especially effective as practical and robust methods to define solution adaptive grids (refs. 51-53) These codes have been used for a variety of flows, both steady and unsteady and in both 2-D and 3-D. Use of this technique significantly improves the accuracy and efficiency of the Navier-Stokes methods. An application of the CSCM method using the adaptive grid is shown in figures 13 and 14 for a 2-D hypersonic inlet (ref. 50). The solution adapted grid is shown in figure 13 and corresponding computed pressure contours on this grid are shown in figure 14. The shock reflection along the lower boundary and the interaction of the expansion waves with the reflected shock are the major features of this flow. The interaction of the expansion fan with the reflected shock results in a curved reflected shock. The predicted pressure recovery behind the reflected shock is critically dependent on accurate resolution of these features. Other applications using solution adaptive grids with Navier-Stokes methods are described in references 54 and 55, and a recent survey of current state of the art in computational aerothermodynamics is given in reference 56.

NONEQUILIBRIUM CHEMISTRY

The development and validation of a computer program to calculate the flow of nitrogen and air in thermal and chemical nonequilibrium is a first step toward the longer range goal of predicting multidimensional flow fields in nonequilibrium air and for hydrogen-air combustion processes. This predictive capability is critical to designing the protective heat shield for the AOTV where radiation heating loads are expected to be severe, and to analyzing scramjet engine performance for the air-breathing propulsion system of TAVs. Thermochemical nonequilibrium reacting gas models have been considered by Park (refs. 27, 28, 57). A computer program identified as "Shock Tube Radiation Program" (STRAP) (ref. 27) has been developed which computes 1-D viscous flows of nitrogen and air in a constant-area duct. By improving existing theories and by introducing several new innovations, differences between the translational and rotational temperature and the vibrational and electron-electronic temperature are considered as are chemical reactions whose rates depend on those two temperatures. The computed nonequilibrium thermodynamic properties have been analyzed using the Nonequilibrium Air Radiation (NEQAIR) (ref. 58) program to determine the spectral radiation characteristics. The resulting radiation characteristics are compared with available experimental data. Shown in figure 15 is a comparison of computed and experimental emission intensity spectra for air behind a normal shock at a velocity of 10 km/sec and pressure of 0.1 torr. The computations were performed using a two-temperature gas model in which the translational and rotational temperatures were equal to one another but different from the vibrational and electron temperatures which were assumed equal to one another. The point behind the shock where the comparison is made is nearly halfway between the onset of the shock and the point downstream where the air is once again in thermal equilibrium. Good agreement is observed between the experimental and the present theoretical data, thus validating the computations and the computer code.

Lee (ref. 59) derived the basic governing equations for the low-density, high-enthalpy flow regimes expected over the heat shields of proposed AOTVs by combining and extending existing theories. The conservation equations are derived from gas kinetic principles and a four-component ionized gas consisting of neutral molecules, neutral atoms, singly ionized ions, and electrons, assuming a continuum flow. The differences among translational-rotational, vibrational, and electron temperatures are accounted for as well as chemical nonequilibrium and electric-charge separation. Expressions for convective and viscous fluxes, transport properties, and the terms representing interactions among various energy modes are explicitly given. The expressions for the rate of electron-vibration energy transfer, which violates the Landau-Teller relation, are derived by solving the system of master equations accounting for the multiple-level transitions. Subsequently, a theoretical study was made (ref. 60) of the electron-impact vibrational excitation rate processes expected in the AOTV flow fields. Semi-empirical quantum-mechanical treatment was adopted to predict the vibrational excitation cross sections and the rate coefficients. The obtained results for e^- collisions with N_2 showed reasonable agreement with available experimental data. The solution to the e^- N_2 vibrational rate equation revealed the unexpectedly slow process to equilibrium which is the result of the diffusion characteristic and multiple-level transitions at high-temperature regions. A modified Landau-Teller-type rate equation and a corresponding relaxation time are suggested which are suitable for numerical calculations relevant to AOTV flow fields.

EXPERIMENTAL PROGRAM

Experimental facilities used for the purpose of code validation include the Ames 3.5-Foot Hypersonic Wind Tunnel which is used for testing generic high-lift configurations at Mach numbers of 5, 7, 10 and 14, the pressurized ballistic ranges which can produce flight speeds up to 27 km/sec and is used to test AOTVs and planetary probes such as the Galileo probe, and the electric arc driven shock tube which can produce nonequilibrium flows at speeds up to 13 km/sec. Flight experiments for both the drag brake and the high-lift configurations are planned for early in the next decade.

Shock Tube

The 24-in. EAST Facility was operated with pressures between 7 and 30 μm of mercury to simulate flight altitudes between 68 to 81 km. Test firings show that: 1) shock velocities in excess of 13 km/sec are achieved at densities equivalent to altitudes of 80 km., 2) the hot driver gas emits radiation in the same pattern as observed in previous higher density, slower shock speed tests, 3) the driver gas does not radiate at unanticipated spectral frequencies, and 4) there is no significant radiation spectra from common impurities such as sodium and iron. This facility will be used to perform basic experiments on thermochemical nonequilibrium with particular emphasis on vibrational energy excitation and nonequilibrium. A description of proposed tests and instrumentation is given by Sharma and Park (ref. 61).

Ballistic Ranges

Two ballistic range facilities at Ames Research Center support hypersonic research (ref. 62), the Hypersonic Free Flight Aerodynamic Facility (HFFAF) and the Pressurized Ballistic Range (PBR). The two facilities compliment each other; each has specific advantages for certain types of tests. Together, they allow testing of a variety of models over a wide range of test conditions. Each facility and associated experiments is described briefly.

Hypersonic Free Flight Aerodynamic Facility

A photograph and schematic of this facility are shown in figure 16. The test section is 23-m long and has 16 orthogonal spark shadowgraph stations evenly spaced (1.52 m) over its length. Kerr-cell shutters are used to produce a sharp model and flow-field image on the film. Four deformable-piston light-gas guns, having bore diameters of 0.71, 1.27, 2.54, and 3.81 cm, are available for launching the model into free flight. Each of these guns can operate to muzzle velocities of about 9 km/sec. A shock tube to provide a countercurrent flow capability is available, but has not been used for recent tests.

Tests in this facility can be conducted from 1 atm to as low as about 20 μm Hg. And tests can be conducted in nontoxic gases other than air, such as CO_2, H_2, He, Kr, and Xe.

Pressurized Ballistic Range

The PBR consists of a large tank that can be pressurized or evacuated and a test section 62-m long. It has 24 orthogonal spark shadowgraph stations irregularly spaced over its length. The station spacing ranges from 2.1 m to 4.2 m. All of the optics are internal to the tank, which imposes a limit on the maximum velocity of the model. Many tests in this facility are conducted with powder gas guns rather than the more sophisticated deformable-piston light-gas guns. The advantages of this facility over HFFAF are threefold: long model trajectory, pressures up to about 6 atm, and highly detailed shadowgraphs.

Galileo Tests

The ballistic ranges at Ames have supported all of the U.S. probe missions to other planets. These include the 1976 Viking Mission to Mars and the 1978 Pioneer Venus Mission. Currently, tests are being conducted on the Galileo probe. The Galileo spacecraft will be launched in the near future and will arrive at Jupiter 2 yr later. The spacecraft consists of two major components, an orbiter which is to orbit Jupiter numerous times, concentrating on close encounters with many of Jupiter's moons, and a probe to enter (and descend through) the atmosphere of Jupiter. The probe will make in situ measurements as it descends through the atmosphere prior to its eventual destruction due to extreme external pressures.

Although the probe aerodynamics were needed initially for design purposes, more accurate aerodynamics are needed in support of the Atmosphere Structure Experiment carried on board the probe. The Atmosphere Structure Experiment is designed to determine the state properties (i.e., density, pressure, temperature) of an unknown planetary atmosphere as functions of altitude from measurements made during the entry and descent of a probe. The experiment consists of a three-axis accelerometer, plus pressure and temperature sensors. During the high-speed portion of the trajectory, from an entry velocity

above 47 km/sec to sonic speed, direct measurements are impractical and accelerometers are used to determine the state properties. This requires the precise knowledge of the probe aerodynamics, in particular the vehicle drag and lift coefficients as functions of Mach number and Reynolds number. The aerodynamic characteristics plus the measured decelerations allow the probe attitude to be determined and the atmospheric density to be deduced. Integration of the density gives the pressure, and the temperature is deduced from the equation of state (given the molecular weight, which is measured by another on-board experiment). The ballistic range facilities are well suited for providing the accurate aerodynamic data over a wide range of conditions.

The Galileo probe is a blunt, 45° cone. During the high-speed part of the entry, severe ablation takes place. As much as 40% of the vehicle mass at entry is expected to be ablated away, mostly in the nose and conical regions, and even the maximum diameter will be significantly decreased. Hence, tests must be conducted not only of the entry configuration but of hypothetical ablated configurations as well.

A typical shadowgraph of a Galileo model in flight obtained in HFFAF is shown in figure 17. The screw on the model base is for attachment to its sabot prior to launch. The vertical wires are plumb bobs on both sides of the facility for reference purposes and the irregular markings are imperfections in the facility windows caused by past impacts of various sorts.

Low Reynolds Number Tests

Ballistic range tests are currently being conducted to precisely define the drag characteristics of the Galileo probe at Reynolds numbers, based on model diameter, of about 500 to 250. The importance of obtaining drag data at these low Reynolds numbers is due to the fact that the drag coefficient is expected to increase markedly as the slip-flow and free-molecule-flow regimes are approached. This dramatic increase in drag coefficient occurs below a Reynolds number of about 1000.

The importance of obtaining drag data at various Reynolds numbers is shown in figure 18. Shown are Pioneer Venus data down to a Reynolds number of about 250. The drag coefficient increases continuously below a Reynolds number of 1 million, but the increase becomes most dramatic below 1000.

AOTV Tests

Ballistic range tests have been conducted for two AOTV configurations; a symmetric configuration and raked elliptic cone. These tests were conducted to: 1) Provide experimental aerodynamic data and good flow-field definition against which computational aerodynamicists could validate their computer codes. 2) Define bow shock-wave shape and shock standoff distance, 3) Investigate flow impingement on afterbody, 4) Compare the aerodynamics of several configurations, 5) Investigate how minor changes in corner geometry affect the flow field, 6) Determine the trim angle of attack of a trimmed vehicle.

A shadowgraph for the symmetric configuration in figure 19 and for the raked elliptic cone in figure 20. These flow visualizations plus drag data from these tests are used for computer code validation.

14

3.5-Ft Hypersonic Wind Tunnel

The current test program in the 3.5-ft hypersonic wind tunnel is focused on a generic all-body (elliptic cross section, delta planform) hypersonic aircraft model. This configuration is representative of airbreathing TAVs now being considered. Flow-visualization (shadowgraphs and surface oil-flow patterns), surface-pressure, surface heat-transfer, and flow-field surveys using probes and nonintrusive lasers will be obtained for this model both with and without control surfaces. Angles of incidence to the free stream will be varied between plus and minus 15° and the free-stream Reynolds number varied between 1.5×10^6 and 25×10^6. Shown in figure 21 is a model with all control surfaces attached. The model has a half angle of 75° and is 1-m long. There are two nose configurations: a sharp nose and a blunted nose. The simple geometrical configuration is easy to define for computer flow codes and can be readily used to evaluate a wide variety of hypersonic flow codes.

Aeroassist Flight Experiment (AFE)

A forthcoming NASA flight experiment called the AFE is planned for early in the next decade. Ames Research Center will participate in this experiment by assimilating a large base of radiometric data for high-altitude, high-velocity, thermochemically nonequilibrated flow conditions. The AFE will be carried to orbit by the space shuttle and then deployed for the atmospheric data pass. Accelerated by an 18,000-lb-thrust solid-rocket motor, the vehicle will enter the atmosphere at nearly 10 km/sec, and then experience approximately 500 sec of aerodynamic deceleration during which a variety of flight data, including radiative and convective heating rates, will be gathered. The vehicle will exit the atmosphere at orbital speed to be recovered by the shuttle orbiter for return to earth for post-flight evaluation. As a preliminary to the design of a radiometer for this experiment, an approximate method for predicting both equilibrium and nonequilibrium radiative surface fluxes has been developed (ref. 63). Spectral results for one trajectory state, a velocity of 10 km/sec at an altitude of 85 km, are shown in figure 22, where the spectral surface flux at a distance of 20.9 cm behind the shock front is plotted as a function of wavelength in the spectral region from 0.2 to 2.0 μm. An inspection of the figure reveals that the spectrum appears to be composed of a background continuum with a color temperature in the range of 7,000° to 8,000° K (based on a flux maximum in the vicinity of 0.4 μm) on which is superimposed a complex structure of molecular bands and broadened atomic lines. The radiation calculation included nine species (O_2, N_2, NO, O, N, N^+, O^+, N_2^+, e^-); some of more apparent band-heads and lines from these species are identified in the figure. These results, and others like them, are used to develop the instrument parameters for the three different types of radiometers proposed for the experiment.

CONCLUDING REMARKS

Aerothermodynamic research underway at NASA Ames has been described. Four research areas are considered synergistically in an effort to mature the enabling technology necessary for the design of the next generation aerospace transporation systems. These four areas include 1) advanced mission and concept studies, 2) computational aerothermodynamic flow-field code development, 3) thermochemical nonequilibrium reacting gas

models, and 4) code-validation experiments. Research in these areas continues in an effort to improve the accuracy and efficiency of predictive methods and our understanding of hypervelocity flows and its effect on aerospace vehicles.

REFERENCES

1. Cooper, D. M.; Jaffe, R. L.; and Arnold, J. O.: Computational Chemistry and Aeroassisted Orbital Transfer Vehicles. AIAA J. Spacecraft and Rockets, vol. 22, Jan. - Feb. 1985, pp. 60-67.

2. Anderson, J. D., Jr.: A Survey of Modern Research in Hypersonic Aerodynamics. AIAA Paper 84-1578, 1984.

3. Graves, R. A., Jr.; and Hunt J. L.: NASA's Hypersonic Fluid and Thermal Physics Program (Aerothermodynamics). AIAA Paper 85-0922, 1985.

4. Lewis, C. H.: Current Status of Computational Aerothermodynamics. AIAA Paper 86-0229, 1986.

5. Walberg, G. D.: A Survey of Aeroassisted Orbital Transfer. AIAA J. Spacecraft and Rockets, vol. 22, Jan.-Feb. 1985, pp. 3-18.

6. Menees, G. P.: Trajectory Analysis of Radiative Heating for Planetary Missions with Aerobraking of Spacecraft. AIAA J. Spacecraft and Rockets, vol. 22, 1985, pp. 37-45.

7. Menees, G. P.: Thermal Protection Requirements for Near-Earth Aeroassisted Orbital Transfer Vehicle Missions. Prog. in Astronaut. and Aeronaut., vol. 96, 1985, pp. 257-285.

8. Menees, G. P.; Park, C.; and Wilson, J. F.: Design and Performance Analysis of a Conical Aerobrake Orbital Transfer Vehicle Concept. Prog. Astronaut. and Aeronaut., vol. 96, 1985, pp. 286-308.

9. Menees, G. P.; Davies, C. B.; Wilson, J. F.; and Brown, K. G.: Aerothermodynamic Heating Analysis of Aerobraking and Aeromaneuvering Orbital Transfer Vehicles. Prog. Astronaut. and Aeronaut., vol. 96, 1985, pp. 338-360.

10. Davies, C. B.; and Park, C.: Aerodynamics of Generalized Bent Biconics for Aero-Assisted, Orbital-Transfer Vehicles. AIAA J. Spacecrafts and Rockets, vol. 22, no. 2, Mar.-Apr. 1985, pp. 104-111.

11. Davies, C. B.; and Park, C.: Optimum Configuration of High-Lift Aeromaneuvering Orbital Transfer Vehicles in Viscous Flow. AIAA Paper No. 85-1059, 1985.

12. Scott, C. D.; Reid, R. C.; Maraia, R. J.; Li, C. P.; and Derry, S. M.: An AOTV Aeroheating and Thermal Protection Study. Prog. Astronaut. and Aeronaut.: Thermal Design of Aeroassisted Orbital Transfer Vehicles, vol. 96, 1985, pp. 309-337.

13. Scott, C. D.; Roberts, B. B.; Nagy, K.; Taylor, P.; Gamble, B. J. D.; Cerimele, C. J.; Kroll, K. R.; Li, C. P.; and Ried, R. C.: Design Study of an Integrated Aeroraking Orbital Transfer Vehicle. NASA TM-58264, 1985.

14. Davies, C. B.; and Park, C.: Aerodynamic and Thermal Characteristics of Modified Raked-Off Cone. AIAA/ASME Paper No. 86-1309, June 1986.

15. Vinopal, T. J.: System Technology Analysis of Aeroassisted Orbital Transfer Vehicles (AOTVs) Low Lift/Drag (0.0-0.75), Final Report. Vol. 1, Part B–Study Results. F180-29222-1, Boeing Aerospace Co., Seattle, WA, 1985.

16. Park, C.: A Survey of Aerobraking Orbital Transfer Vehicle Design Concepts. AIAA Paper No. 87-0514, Jan. 1987

17. Park, C.: Theory of Idealized Two-Dimensional Ballute in Newtonian Hypersonic Flow. AIAA Paper No. 86-0301, Jan. 1986.

18. Brown, K. G.: Chemical and Thermal Nonequilibrium Heat-Transfer Analysis for Hypervelocity, Low Reynolds Number Flow. Prog. Astronaut. and Aeronaut., vol. 103, 1986, pp. 445-477.

19. Menees, G. P.: Design and Performance Analysis of an Aeromaneuvering Orbital-Transfer Vehicle Concept: 36th Congress of the International Astronautical Federation, IAF-85-139, Stockholm, Sweden, October 7-12, 1985.

20. Tauber, M. E.; and Yang, L.: Performance Comparisons of Maneuvering Vehicles. AIAA Paper No. 87-2490, August 1987.

21. Tauber, M. E.; Menees, G. P.; and Adelman, H. G.: Aerothermodynamics of Transatmospheric Vehicles. AIAA/ASME Paper No. 86-1257, June 1986.

22. Tauber, M. E.; and Adelman, H. G.: The Thermal Environment of Transatmospheric Vehicles. AIAA Paper No. 87-1514, June 1987.

23. Green, M. J.; Budnick, M. P.; Yang, L.; and Chiasson: Supporting Flight Data Analysis for Space Shuttle Orbiter Experiments at NASA Ames Research Center. AIAA Paper No. 83-1532, June 1983.

24. Green, M. J.; Moss, J. N.; and Wilson, J. F.: Aerothermodynamic Environment and Thermal Protection for a Titan Aerocapture Vehicle. AIAA Paper No. 84-1717, June 1984.

25. Green, M. J.; Balakrishnan, A.; and Swenson, B. L.: Aerothermodynamic Environment for a Titan Probe with Deployable Decelerator. AIAA Paper No. 85-1063, June 1985.

26. Balakrishnan, A.; Park, C.; and Green, M. J.: Radiative Viscous Shock Layer Analysis of Fire, Apollo, and PAET Flight Data. Prog. Astronaut. and Aeronaut., vol. 103, 1986, pp. 514-540.

27. Park, C.: Convergence of Computation of Chemical Reacting Flows. Prog. Astronaut. and Astronaut., vol. 103, 1986, pp. 478-513.

28. Park, C.: Assessment of Two-Temperature Kinetic Model for Dissociating and Weakly-Ionizing Nitrogen: AIAA/ASME Paper No. 86-1347, June 1986.

29. Menees, G. P.; Brown, K. G.; Wilson, J. F.; and Davies, C. B.: Aerothermodynamic Heating and Performance Analysis of a High-Lift Aeromaneuvering AOTV Concept. AIAA Paper No. 85-1060, June 1985.

30. Park, C.: Calculation of Nonequilibrium Radiation in the Flight Regimes of Aeroassisted Orbital Transfer Vehicles. Prog. Astronaut. and Aeronaut., vol. 96, 1985, pp. 395-418.

31. Park, C.: Radiation Enhancement by Nonequilibrium in Earth's Atmospher. AIAA J., vol. 22, no. 1, Jan.-Feb. 1985, pp. 27-36.

32. Eberhardt, S.; and Brown, K. G.: A Shock Capturing Technique for Hypersonic, Chemically Relaxing Flows," AIAA Paper No. 86-0231, Jan. 1986.

33. Eberhardt, S.; and Palmer, G. E.: A Two-Dimensional, TVD Numerical Scheme for Inviscid, High Mach Number Flows in Chemical Equilibrium. AIAA/ASME Paper No. 86-1284, June 1986.

18

34. Palmer, G. E.: An Implicit Flux-Split Algorithm to Calculate Hypersonic Flowfields in Chemical Equilibrium: AIAA Paper No. 87-1580, June 1987.

35. Yang, J. Y.: A Hybrid Upwind Scheme for the Computation of Shock-On-Shock Interaction Around Blunt Bodies. 10th International Conference on Numerical Methods in Fluid Dynamics, Beijing, China, June 1986.

36. Balakrishnan, A.; Davy, W. C.; and Lombard, C. K.: Real-Gas Flowfields about Three-Dimensional Configurations. J. Spacecraft and Rockets, vol. 22, no. 1, Jan.-Feb. 1985, pp. 46-50.

37. Gordon, S.; and McBride, B. J.: Computer Program for Calculation of Complex Chemical Equilibrium Compositions, Rocket Performance. NASA SP-273, 1976.

38. Lyubimov, A. N.; and Rusanov, V. V.: Gas Flows Past Blunt Bodies Part I. Calculation Method and Flow Analysis. NASA TT F-714, Feb. 1973.

39. Rakich, J. V.; Venkatapathy, E.; Tannehill, J. C.; and Prabhu, D.: Numerical Solution of Space Shuttle Orbiter Flowfield. AIAA J. Spacecraft and Rockets, vol. 21, no. 1, Jan.-Feb. 1984, pp. 9-15.

40. Balakrishnan, A.: Computation of a Viscous Real Gas Flowfield for the Space Shuttle Orbiter. AIAA Paper No. 84-1748, June 1984.

41. Prabhu, D. K.; and Tannehill, J. C.: Numerical Solution of Space Shuttle Orbiter Flowfield Including Real-Gas Effects. AIAA J., vol. 21, no. 1, Jan.-Feb. 1984, pp. 9-15.

42. Prabhu, K. D.; Tannehill, J. C.; and Marvin, J. G.: A New PNS Code for Chemical Nonequlibrium Flows. AIAA Paper No. 87-0284, Jan. 1987.

43. Prabhu, K. D.; Tannehill, J. C.; and Marvin, J. G.: A New PNS Code for Three-Dimensional Chemically Reacting Flows. AIAA Paper No. 87-1472, 1987.

44. Blottner, F. G.; Johnson, M.; and Ellis, M.: Chemically Reacting Viscous Flow Program for Multi-Component Gas Mixtures. Report No. SC-RR-70-754, Sandia Laboratories, Albuquerque, NM, Dec. 1971.

45. Green, M. J.; Davy, W. C.; and Lombard, C. K.: CAGI2 - A CSCM Based Procedure for Flow of an Equilibrium Chemically Reacting Gas," AIAA Paper No. 85-0927, June 1985.

46. Green, M. J.: Numerical Simulation of Hypersonic, Axisymmetric Flowfields. AIAA/ASME Paper No. 86-1285, June 1986.

47. Lombard, C. K.; Venkatapathy, E.; and Bardina, J.: Forebody and Baseflow of a Dragbrake OTV by an Extremely Fast Single Level Implicit Algorithm. AIAA Paper No. 84-1699, June 1984.

48. Bardina, J.; Venkatapathy, E.; and Lombard, C. K.: Two Dimensional and Axisymmetric Heat-Transfer Results with the CSCM-S Upwind Implicit Algorithm. Prog. in Astronaut. and Aeronaut., vol. 103, 1986, pp. 596-619.

49. Lombard, C. K.; Luh, C.-C; Nagaraj, N.; Bardina, J.; and Venkatapathy, E.: Numerical Simulation of Backward Step and Jet Exhaust Flows. AIAA Paper No. 86-0432, Jan. 1986.

50. Venkatapathy, E.; Palmer, G. E.; Deiwert, G. S.; and Lombard, C. K.: An Efficient Adaptive Patched Grid Gas Dynamic Solver for Complex Flows. AIAA/ASME Paper No. 86-1288, June 1986.

51. Nakahashi, K.; and Deiwert, G. S.: A Practical Adaptive-Grid Methods for Complex Fluid-Flow Problems. NASA TM 85989, June 1984.

52. Nakahashi, K.; and Deiwert, G. S.: A Self-Adaptive-Grid Method with Application to Airfoil Flow. AIAA Paper No. 85-1525, July 1985.

53. Nakahashi, K.; and Deiwert, G. S.: Three-Dimensional Adaptive Grid Method. AIAA J., vol. 24, no. 6, June 1986, pp. 948-954.

54. Deiwert, G. S.; Andrews, A. E.; and Nakahashi, K.: Theoretical Analysis of Aircraft Afterbody Flow. AIAA Paper No. 84-1524, June 1984.

55. Deiwert, G. S.; Rothmund, J. J.; and Nakahashi, K.: Simulation of Complex Three-Dimensional Flows. NASA TM 86773, July 1985.

56. Deiwert, G. S.; and Green, M. J.: Computational Aerothermodynamics. AAS Paper No. 86-350, Oct. 1986.

57. Park, C.: Problems of Rate Chemistry in the Flight Regimes of Aeroassisted Orbital Transfer Vehicles. Prog. Astronaut. and Aeronaut., vol. 96, 1985, pp. 511-537.

58. Park, C.: Nonequilibrium Air Radiation (NEOAIR) Program: User's Manual. NASA TM 86707, July 1985.

59. Lee, J. H.: Basic Governing Equations for the Flight Regimes of Aeroassisted Orbital Transfer Vehicles. Prog. Astronaut. and Aeronaut., vol. 96, 1985, pp. 3-53.

60. Lee, J. H.: Electron-Impact Vibrational Excitation Rates in the Flow Field of Aeroassisted Orbital Transfer Vehicles. AIAA Paper No. 85-1035, June 1985.

61. Sharma, S.; and Park, C.: A Survey of Simulation and Diagnostic Techniques for Hypersonic Nonequilibrium Flows. AIAA Paper No. 87-0406, Jan. 1987

62. Intrieri, P. F.; and Kirk, D. B.: High-Speed Aerodynamics of Several blunt-Cone Configurations. AIAA Paper No. 86-0300, Jan. 1986.

63. Davy, W. C.; Park, C.; Arnold, J. O.; and Balakrishnan, A.: Radiometer Experiment for the Aeroassist Flight Experiment. AIAA Paper No. 85-0967, June 1985.

Table I

RATINGS OF FIVE AEROBRAKING ORBITAL TRANSFER VEHICLE DESIGN CONCEPTS

OO = VERY GOOD, O = GOOD, X = BAD, XX = VERY BAD

	BALLUTE	CONICAL LIFTING-BRAKE	RAKED ELLIPTIC-CONE	LIFTING-BODY	RAKED SPHERE-CONE
NAVIGABILITY	XX	O	O	OO	O
STABILITY AND CONTROL	XX	O	XX	OO	OO
BASE FLOW IMPINGEMENT	OO	O	XX	O	O
RADIATIVE HEATING	XX	X	OO	OO	OO
CONVECTIVE HEATING	XX	OO	O	X	O
FRUSTRUM EDGE HEATING	OO	O	X	X	O
ABORT AND MULTIPLE PASS	XX	O	XX	O	O
TRANSPORTATION AND CONSTRUCTION	OO	X	O	O	O
PAYLOAD/WEIGHT RATIO	OO	X	O	?	O
OVERALL RATING	XX	O	X	?	OO
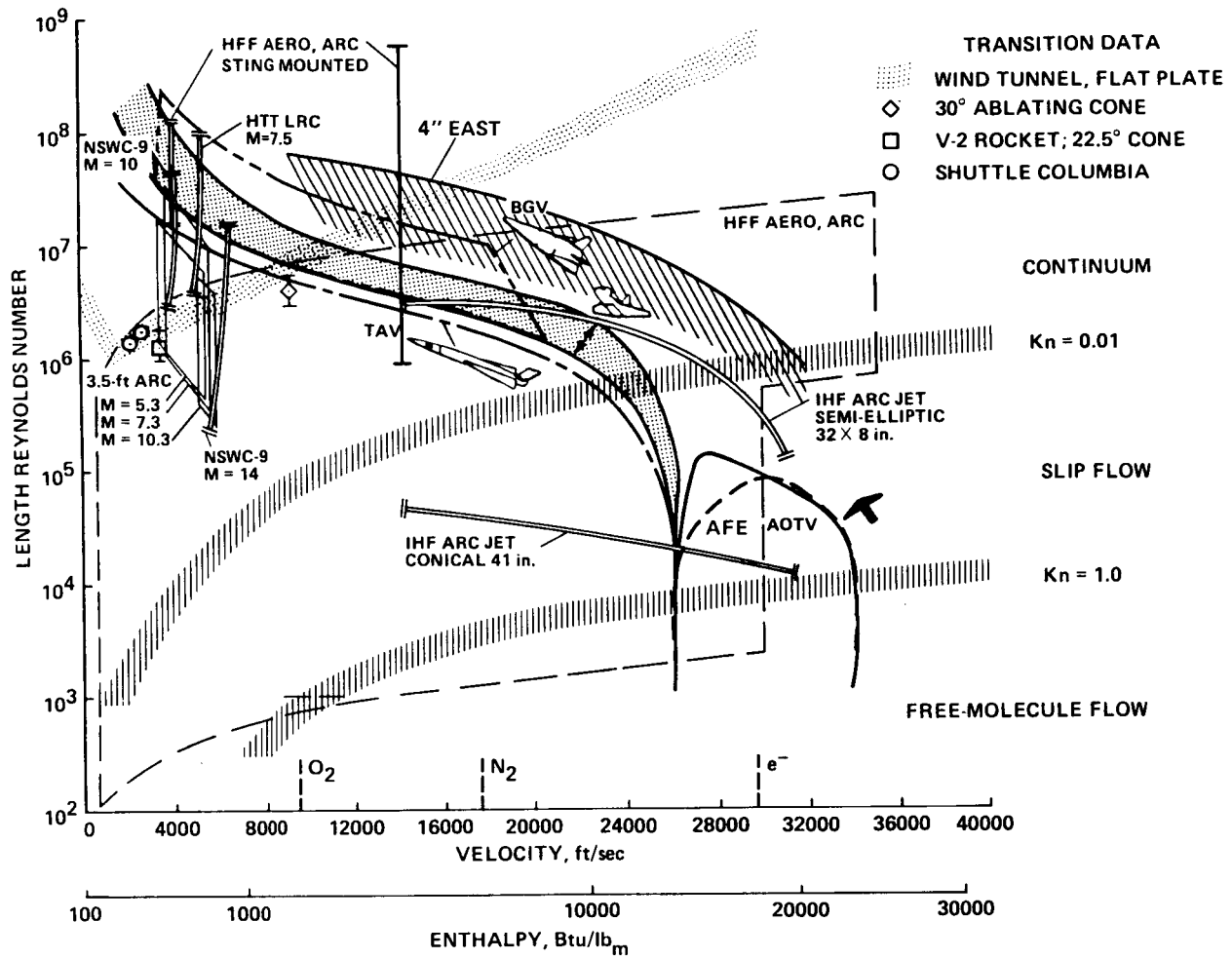
Figure 1.- Flight-domain simulation capability.
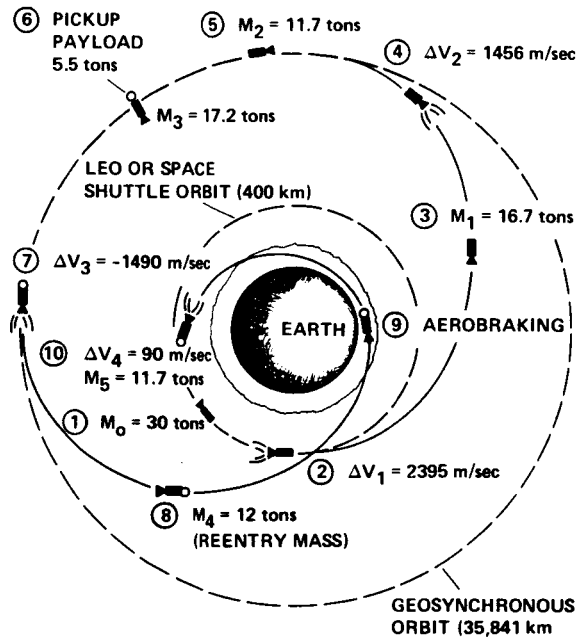
Figure 2.- Mission schematic for AOTV in coplanar maneuver between LEO and GEO. (Masses computed for ip = 420 sec.)

(a) SIDE VIEW

9.1 m

CARGO BAY

BASE FLOW CLEARANCE ANGLE = 25°

REFERENCE FORCE LINE

LH$_2$

6.0 m

WIND VECTOR

LH$_2$

13.1 m

LO$_x$

LH$_2$

MAIN FUEL TANKS

PROTECTIVE SHROUD

CARGO BAY

LH$_2$

LO$_x$

LO$_x$

LH$_2$

AUXILIARY FUEL TANKS

AEROBRAKE HEAT SHIELD

OPEN ⎱ CARGO-BAY
CLOSED ⎰ SHIELDS

THRUST LINES

11.9 m

ROCKET ENGINES WITH TELESCOPIC EXTENSION

(c) BOTTOM VIEW   HATCH DOOR
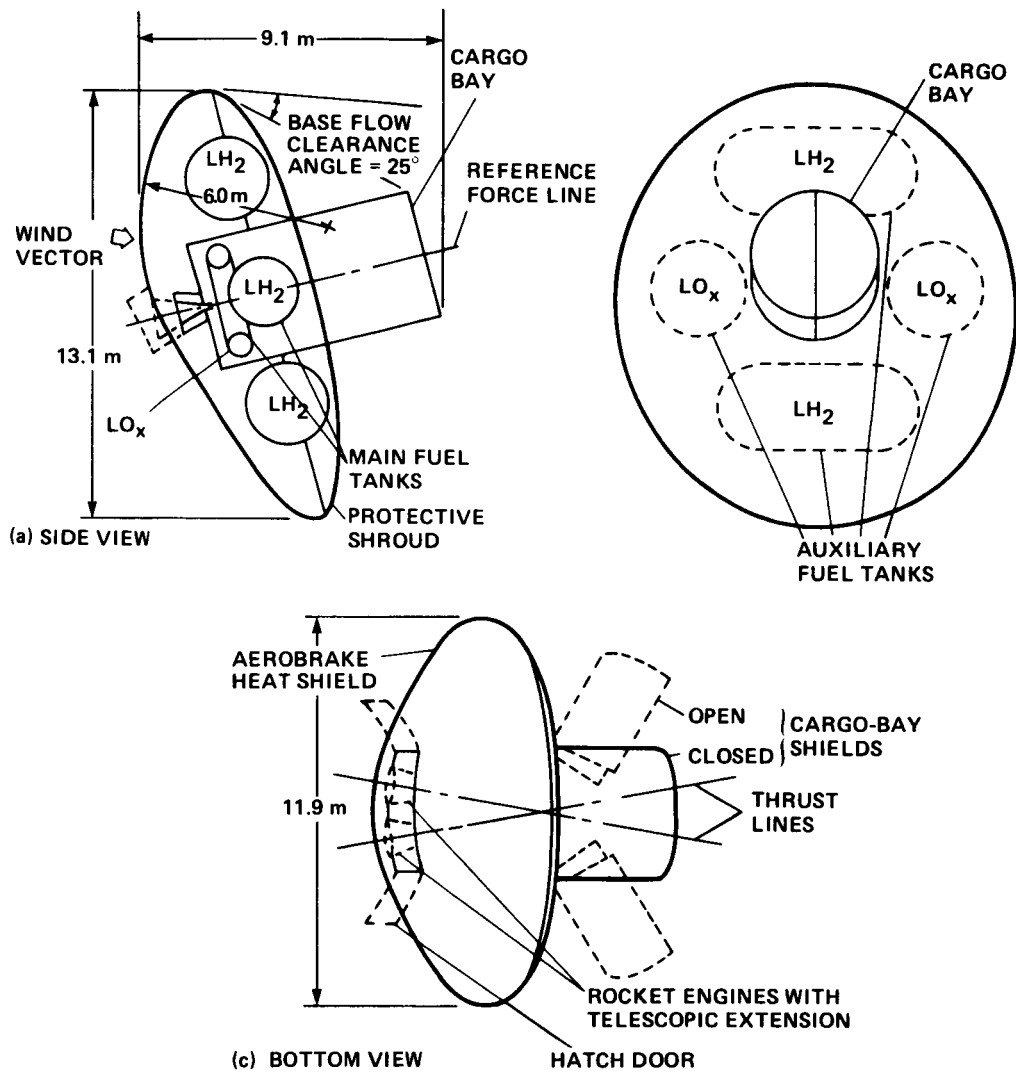
Figure 3.-   Overall AOTV configuration employing the sphere-cone aerobrake.
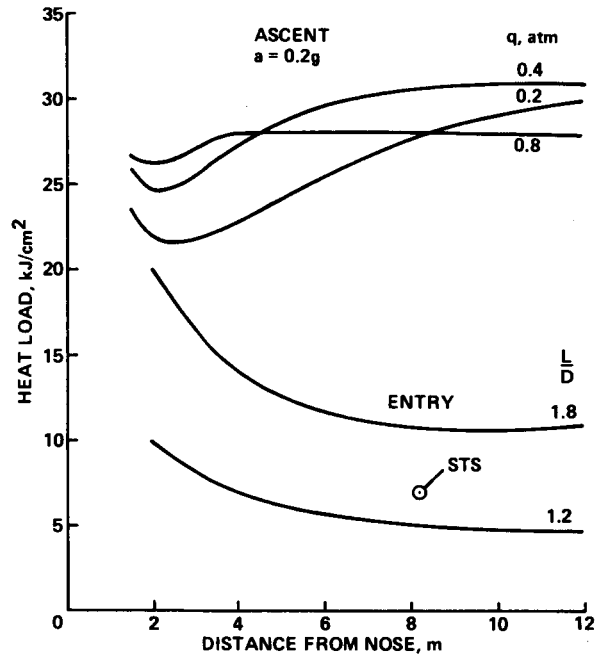
Figure 4.- Total heat loads on generic TAV windward centerline.
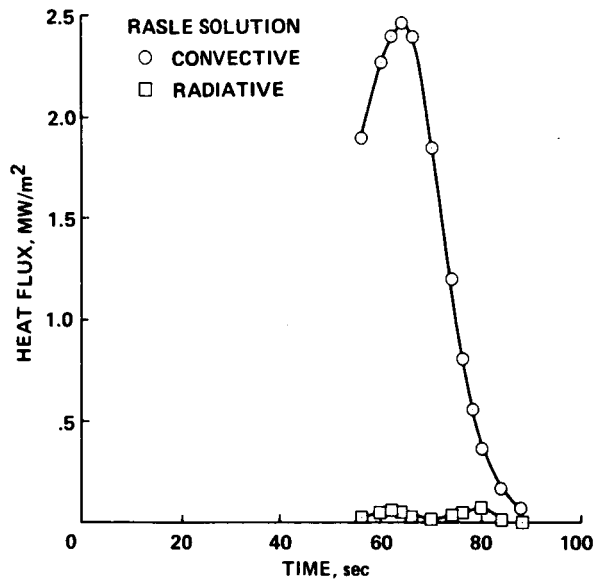
Figure 5.- Heating histories at the stagnation point $(S/R_n = 0)$.
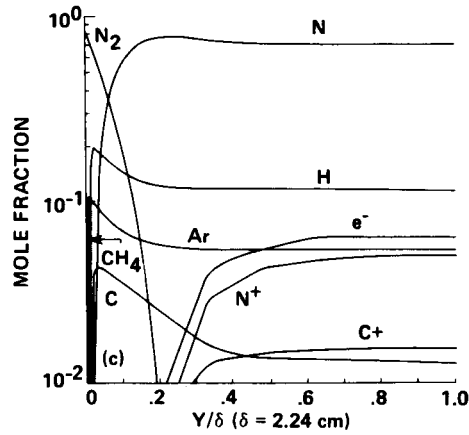
Figure 6.- Shock-layer structure during peak heating along stagnation streamline - chemical species profiles.
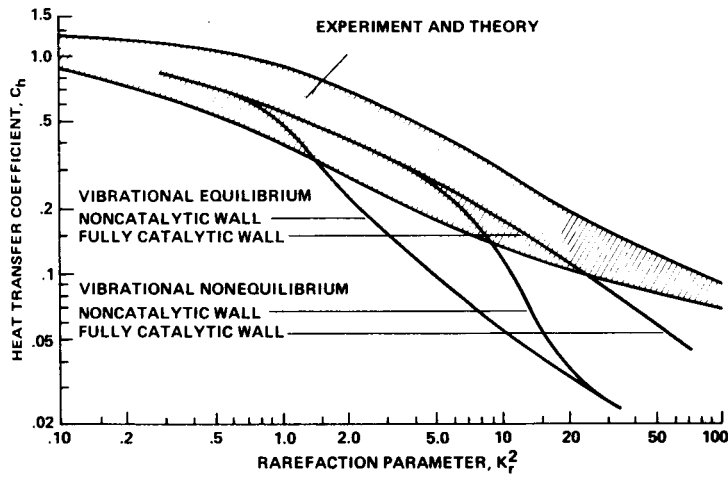
Figure 7.- Convective heat-transfer rate correlation.
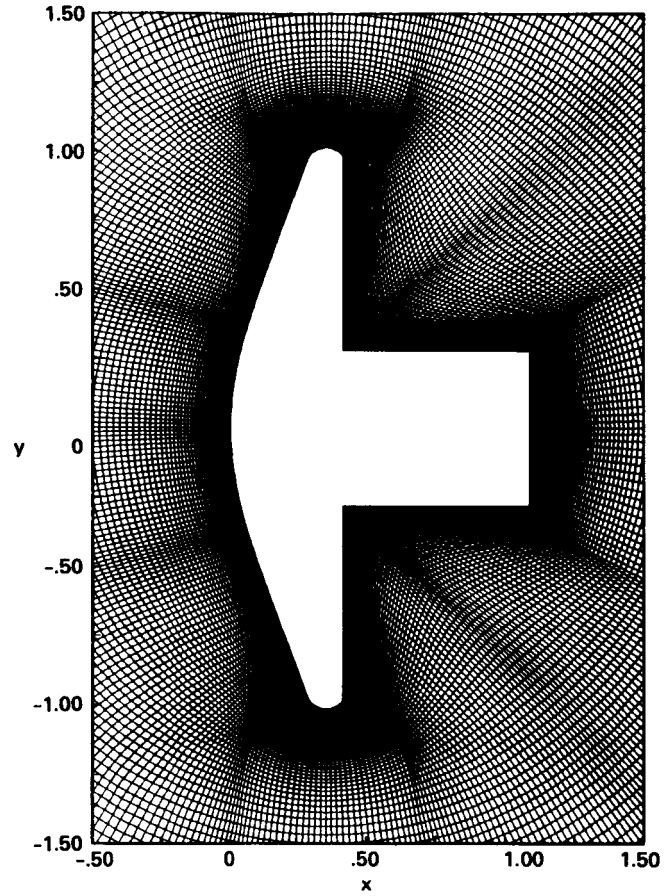
Figure 8.-   Geometry and grid for two-dimensional AOTV flow-field simulation.
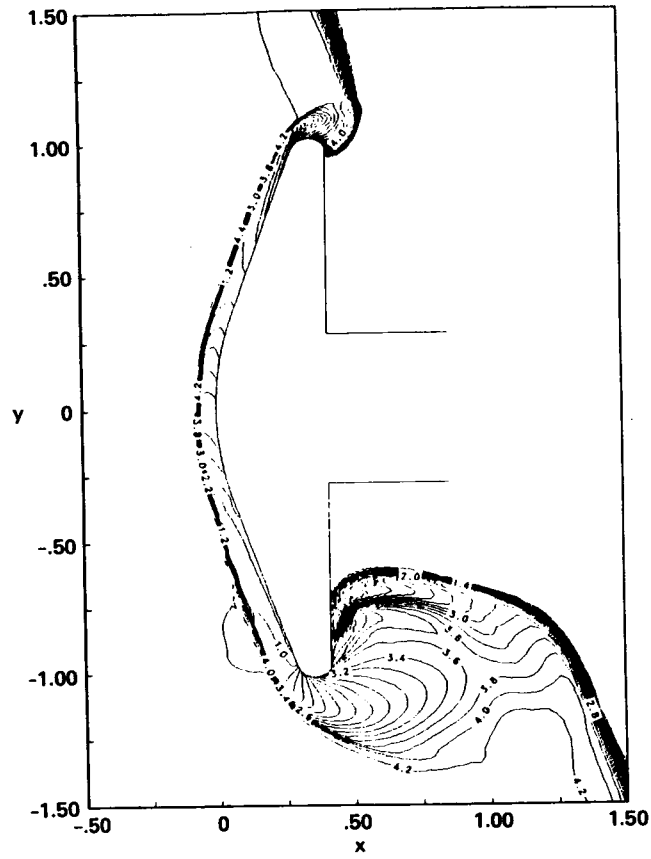
Figure 9.- Computed mach contours for two-dimensional AOTV shape. $M_\infty = 30$, $\alpha = 15°$, $\gamma = 1.1$.
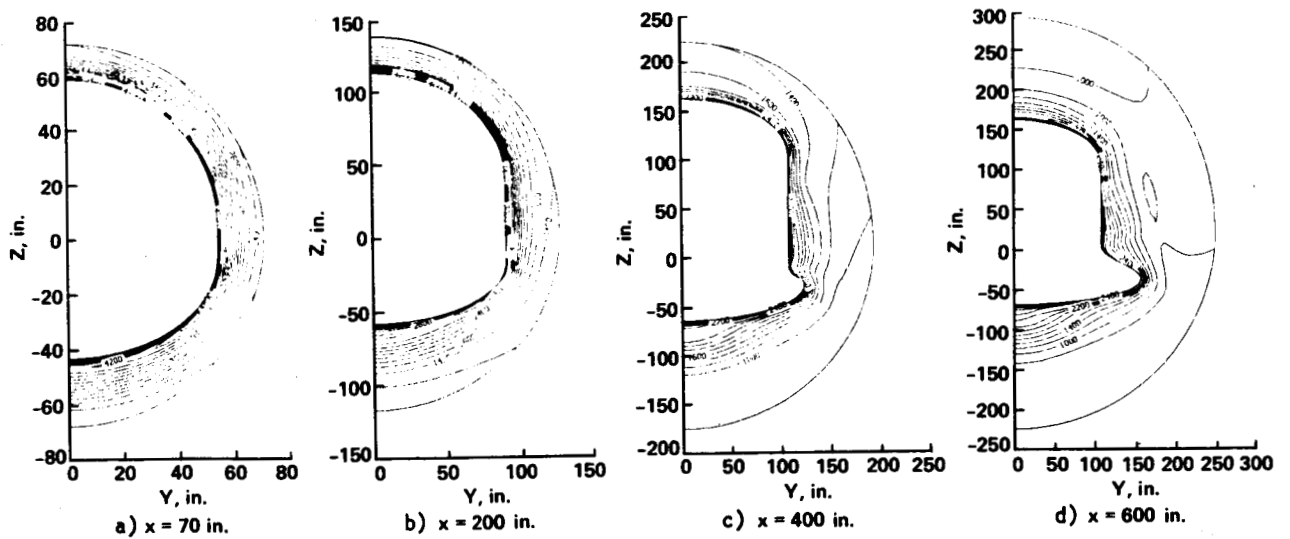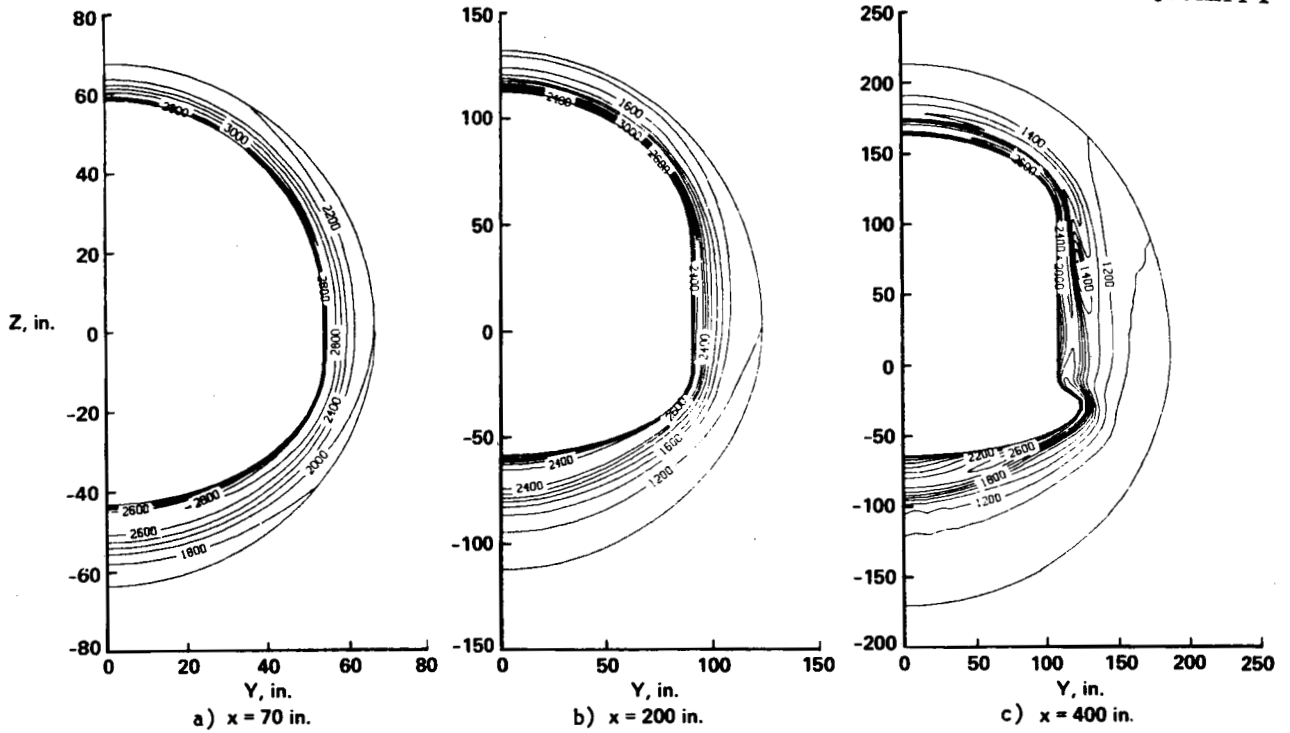
Figure 10.- Comparison of equilibrium and ideal air temperature distributions at several cross-sections of the space shuttle orbiter. $M_\infty = 13$, $H = 55.8$ km. a) Equilibrium air; b) Ideal air.

29
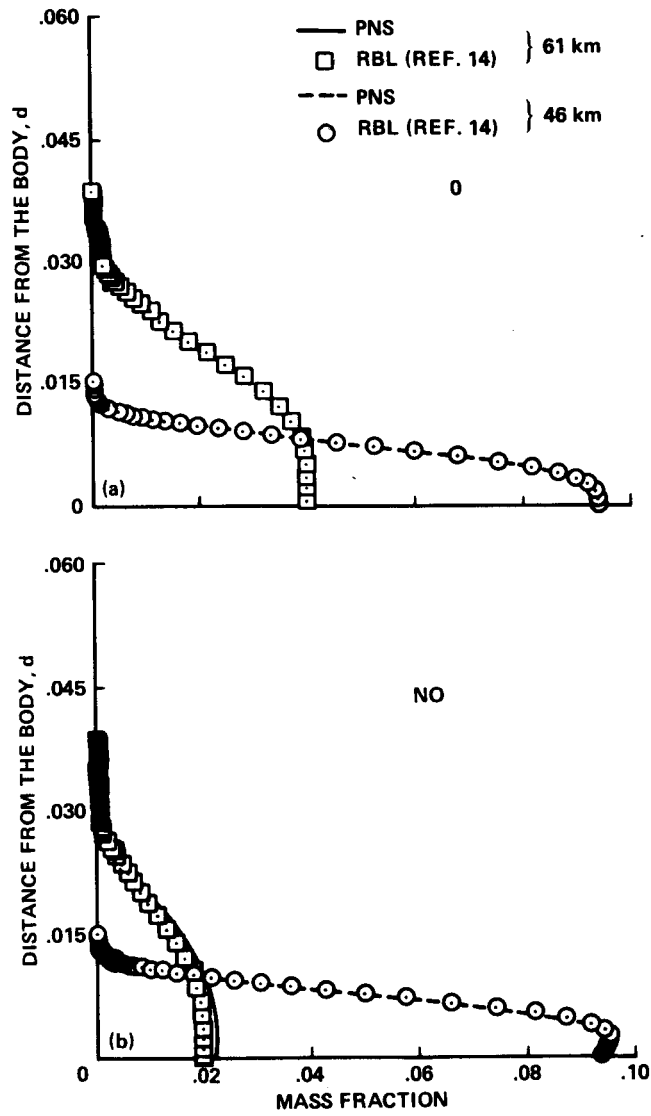
Figure 11.- Computed species mass-fraction profiles in the shock layer of a 10° cone. $V_\infty = 8.1$ km/sec. a) Oxygen mass fraction; b) Nitric oxide mass fraction.
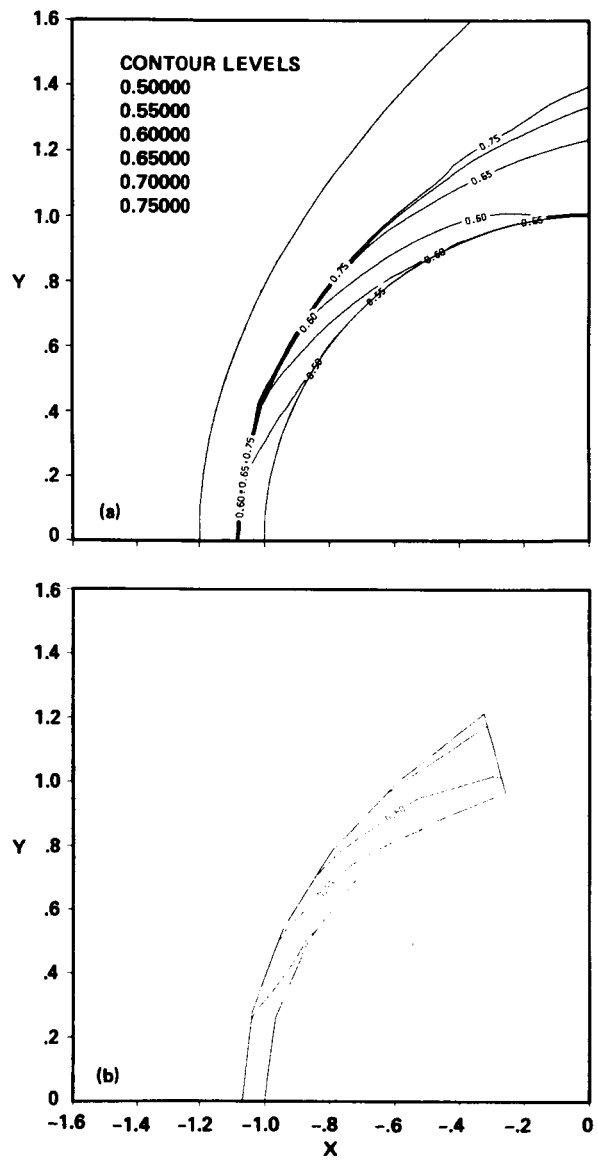
Figure 12.- Comparison of N_2 mole-fraction contours over hemisphere nose. $M_\infty = 20$. a) CAGI2 solution; b) Solution from reference 38.
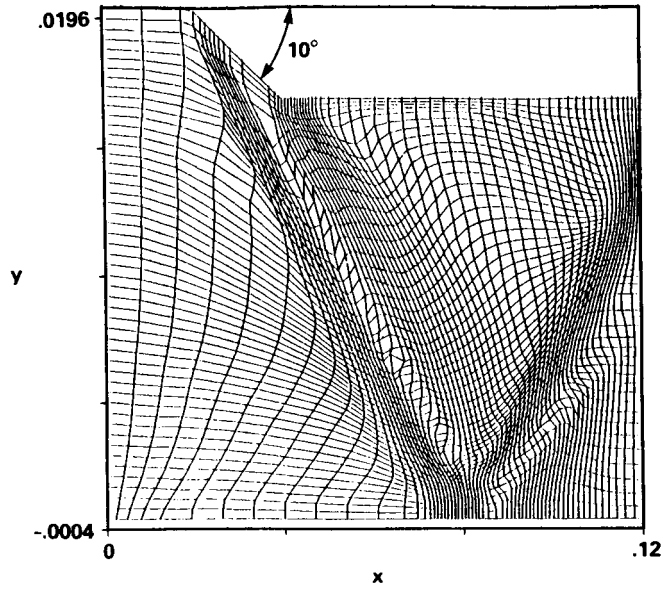
Figure 13.- Solution-adapted hypersonic inlet grid - 10° wedge. (Note unequal scales.)
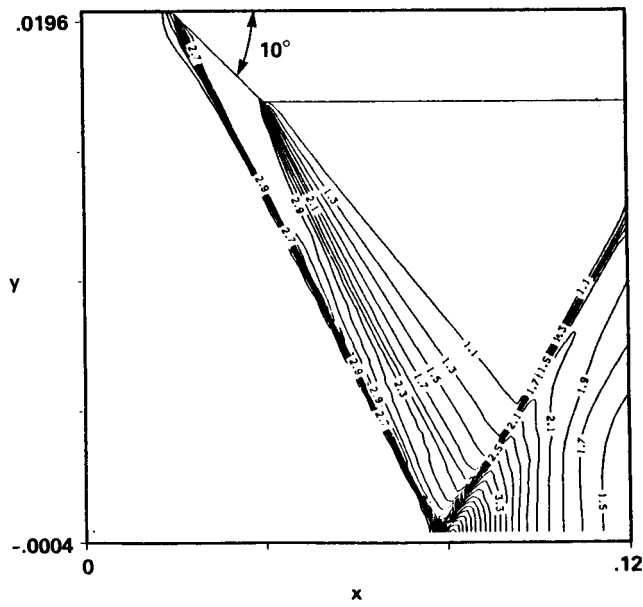
Figure 14.- Computed isobars for hypersonic inlet using solution adapted grid. $M_\infty = 5.0$.
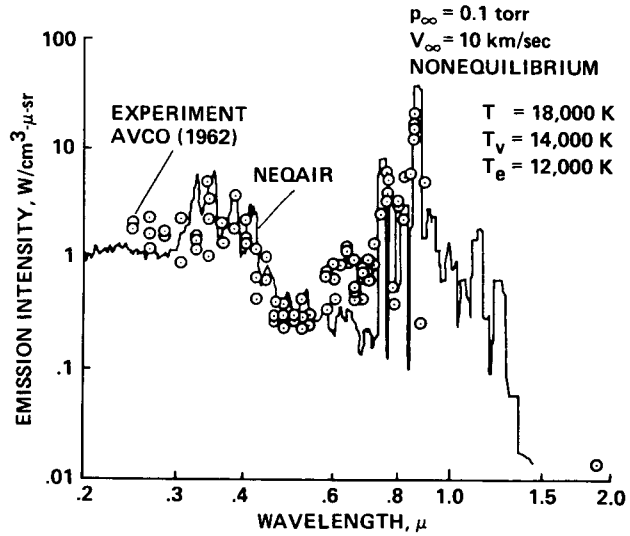
Figure 15.- Comparison between calculated and measured spectra behind a plane normal shock wave.
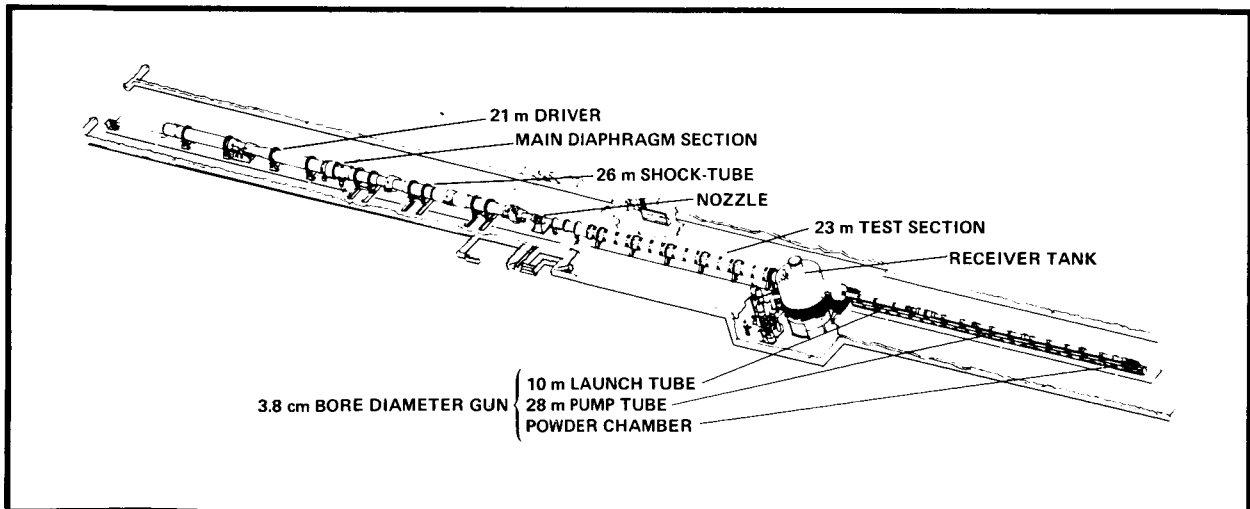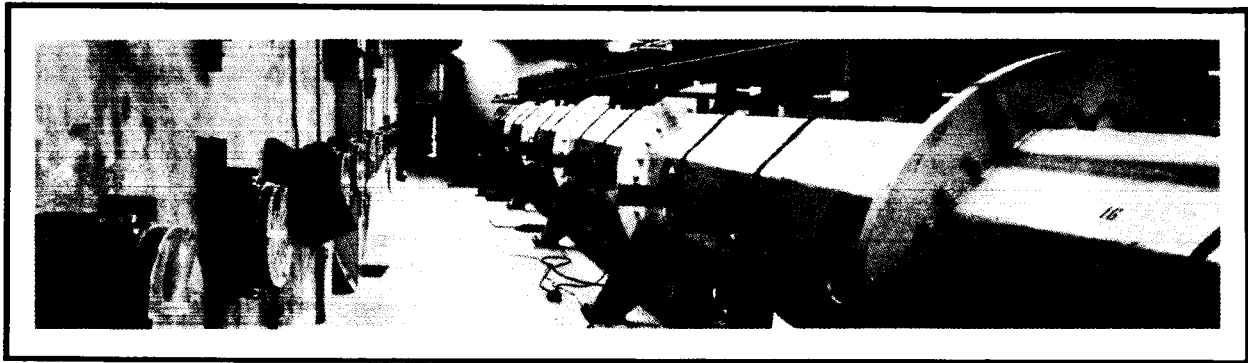
Figure 16.- Hypersonic Free Flight Aerodynamic Facility.

33
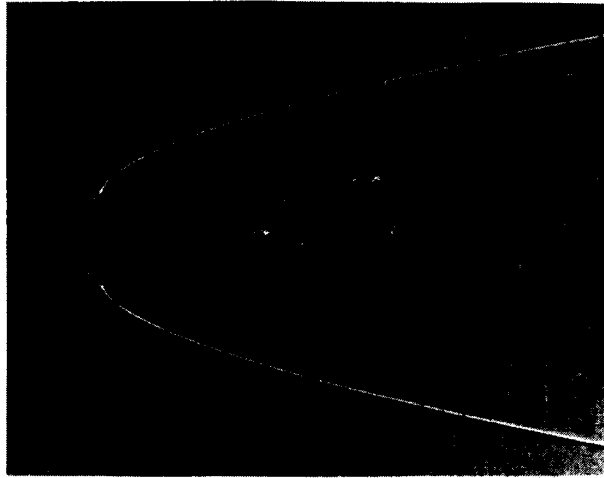
Figure 17.- Shadowgraph of Galileo Probe. $M_\infty = 14$, $Re_d = 100,000$.

VELOCITY ~ 4600 m/sec
TEST GAS – CO_2
ANGLE OF ATTACK = 0°

c_D

REYNOLDS NUMBER (BASED ON d)
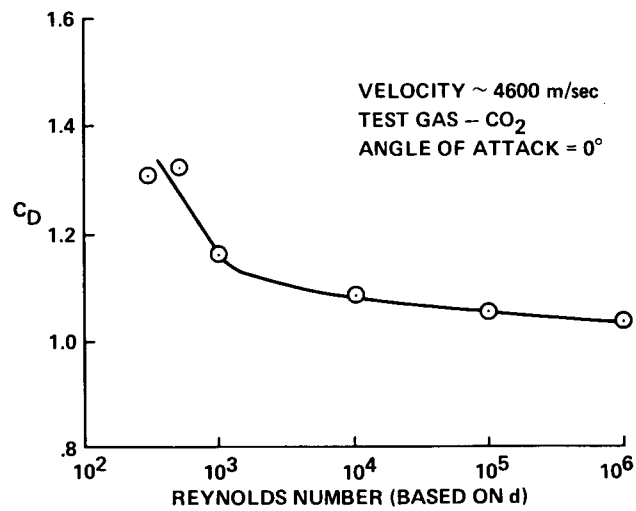
Figure 18.- Effect of Reynolds number on drag-character characteristics of Pioneer Venus.

34
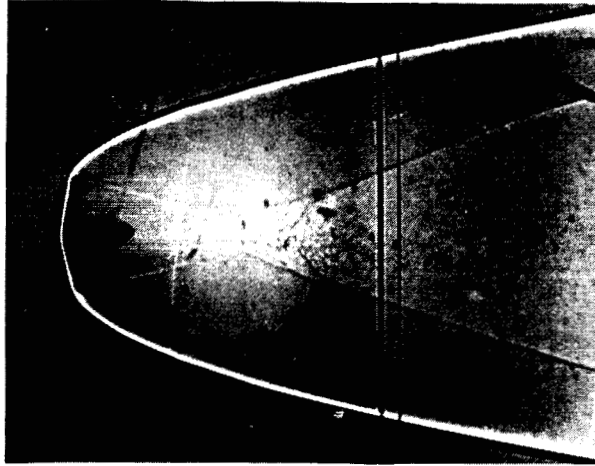
Figure 19.- Shadowgraph of symmetric AOTV.
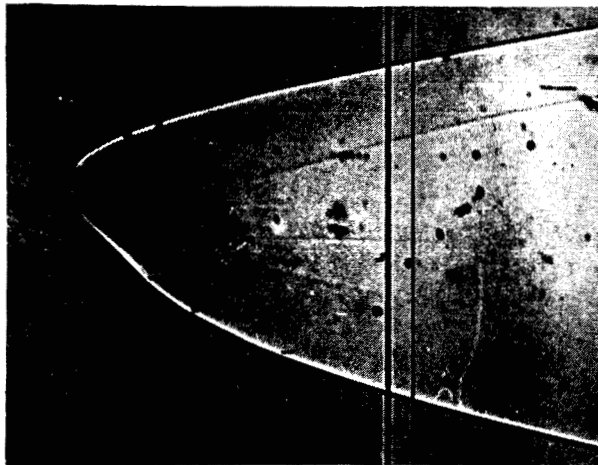
Figure 20.- Shadowgraph of AFE model.
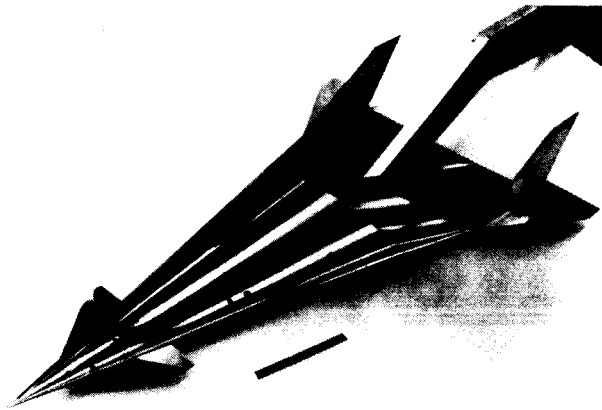
Figure 21.-   Generic all-body hypersonic aerospace plane model.   75° half-angle delta with elliptic cross section.

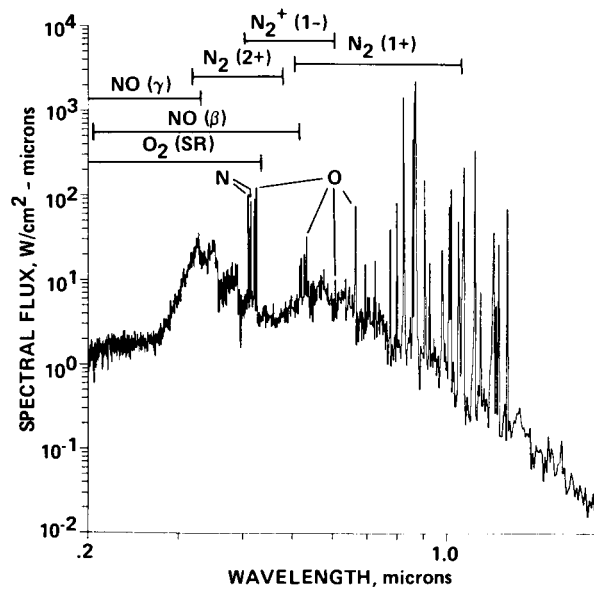Figure 22.-   Nonequilibrium-flow spectral flux: Shock-layer Depth = 20.9 cm.

NASA
National Aeronautics and
Space Administration

Report Documentation Page

1. Report No. NASA TM 89439	2. Government Accession No.	3. Recipient's Catalog No.

4. Title and Subtitle	5. Report Date
Aerothermodynamics Research at NASA Ames Research Center	September 1987
	6. Performing Organization Code

7. Author(s)	8. Performing Organization Report No.
George S. Deiwert	A-87149

10. Work Unit No. 506-40-11

9. Performing Organization Name and Address	11. Contract or Grant No.
Ames Research Center Moffett Field, CA 94035	

13. Type of Report and Period Covered Technical Memorandum

12. Sponsoring Agency Name and Address	14. Sponsoring Agency Code
National Aeronautics and Space Administration Washington, DC 20546-0001	

15. Supplementary Notes

Point of Contact: George S. Deiwert, Ames Research Center, M/S 230-2, Moffett Field, CA 94035
(415)694-6198 or FTS 464-6198

16. Abstract

   Research activity in the aerothermodynamics branch at the NASA Ames Research Center is reviewed. Advanced concepts and mission studies relating to the next generation aerospace transportation systems are summarized and directions for continued research identified. Theoretical and computational studies directed at determining flow fields and radiative and convective heating loads in real gases are described. Included are Navier-Stokes codes for equilibrium and thermochemical nonequilibrium air. Experimental studies in the 3.5-ft hypersonic wind tunnel, the ballistic ranges and the electric arc driven shock tube are described. Tested configurations include generic hypersonic aerospace plane configurations, aeroassisted orbital transfer vehicle shapes and Galileo probe models.

17. Key Words (Suggested by Author(s))	18. Distribution Statement
Aerothermodynamics Transatmospherics AOTVs	Unclassified – Unlimited Subject Category – 12

19. Security Classif. (of this report)	20. Security Classif. (of this page)	21. No. of pages	22. Price
Unclassified	Unclassified	40	A03